MICHIGAN STATE UNIVERSITY

CYCLOTRON LABORATORY

"STRIPPING" REACTION IN HEAVY ION PROJECTILE DISSOCIATION -AN EXTENDED SERBER MODEL-

H. UTSUNOMIYA

FEBRUARY 1985

MSUCL-508

MSUCL-508
February 1985

"Stripping" Reaction in Heavy Ion Projectile Dissociation

-an extended Serber model-

H. Utsunomiya

National Superconducting Cyclotron Laboratory, Michigan State University, East Lansing, Michigan 48824

The opaque Serber model is extended for "stripping" reaction in heavy ion projectile dissociation by incorporating a critical distance between constituent clusters in the projectile. This model describes the higher energy part of the fragment inclusive spectra. The results are discussed in comparison with the local-momentum PWBA calculations by McVoy and Nemes and with the Friedman model.

Heavy ion quasi-elastic collisions at intermediate energies, 10 to 100 MeV per nucleon, have attracted considerable interest as reaction mechanisms are unknown. An interesting feature that has appeared[1,2] is that the momentum distribution widths of the quasi-elastic component grow across the intermediate energies and approach the limiting values for the projectile fragmentation at relativistic energies.[3] The proposed origins of the growing widths are a change in reaction mechanism from transfer to fragmentation[4] or the effects of the Coulomb field, usually called Coulomb distortion[5].

In this work, we extend an opaque version of the Serber model[6] to study "stripping" reaction in heavy ion projectile dissociation. Apart from its conventional usage, the stripping reaction means here that the unobserved fragment is removed from the projectile and undergoes a subprocess between the fragment and target that can be anything from inelastic scattering to fusion. The model was applied to data available for dissociation of 280 MeV-^{14}N by ^{165}Ho, 218 MeV- and 315 MeV-^{16}O by ^{208}Pb, and ^{20}Ne by ^{197}Au at various energies from E/A=7.5 MeV to 20 MeV. The extended Serber model gives similar results to the local-momentum plane-wave Born approximation (LMPWBA) of McVoy and Nemes[4]. That is, only higher energy part of experimental inclusive spectra can be attributed to the stripping reaction. However, the extended Serber model

predicts narrower widths of the momentum distibution than the Friedman model[5].

The Serber model represents an intuitive picture of projectile breakup. Its application was originally limited to breakup of light elements such as deuterons[6] and later ^{3}He and α[7,8] primarily because the model employes a Yukawa[6,7] or Eckart[8] wave function. In addition, the spatial size of the constituents is ignored in these calculations. In order to treat heavy ion projectile dissociation within the framework of the Serber model it is necessary to extend the simple model.

Consider dissociation of a heavy ion, a, into its constituents, b and x, the observed and unobserved fragments, respectively. The intrinsic momentum distribution of b in the projectile is given by the square of the Fourier transform $\psi(\vec{p})$ of the relative wave function $\psi_{b-x}(\vec{r})$ of b and x in a. Let us now introduce a critical distance between b and x in the projectile, outside of which the clusters are well defined and inside of which they cease to exist. The physical meaning of R_c is that the constituents loose their identities or, in other words, dissolve into each other when they are closer than R_c. Assuming the target is opaque to the projectile clusters, we require that b misses the target and continues its flight as a spectator but x strikes and is eliminated from the quasi-elastic "flux". Therefore, the subprocess between x and the target ranges from scattering with large inelasticity to fusion. The Fourier transformation for the stripping

reaction is made under the geometrical requirement, maintaining the distance between b and x greater than or equal to R_c. A detailed discussion of the Fourier transformation is presented in Appendix A. If we take a Yukawa form of wave function at $r \geq R_c$, i.e.,

$$\psi_{b-x}(\vec{r}) \propto \frac{e^{-\alpha r}}{r} \quad , \tag{1}$$

where $\alpha=(2\mu\varepsilon)^{1/2}/\hbar$ with the reduced mass, μ, and separation energy, ε, of the fragment from the projectile, then the parallel momentum distribution, $w(p_{//})$, of b is given by

$$w(p_{//}) = \left|\psi(p_{//})\right|^2 \propto \frac{e^{-2\frac{R_c}{\hbar}(\alpha^2\hbar^2 + p_{//}^2)^{1/2}}}{(\alpha^2\hbar^2 + p_{//}^2)^{5/2}} \quad . \tag{2}$$

The double differential cross section $(d^2\sigma/d\Omega_b dE_b)_{//}$ is given by

$$\left(\frac{d^2\sigma}{d\Omega_b dE_b}\right)_{//} \propto A_b P_b W(P_{//}) \quad . \tag{3}$$

Here, A_b is mass number of b, and $p_{//}$ is the momentum of b parallel to the projectile, which is given by $p_{//} = p_b - p_o$ with the laboratory

momentum p_b and the momentum p_o due to the incident motion of the projectile. A general expression of the double differential cross section at angle θ is given in Appendix B.

The remaining problem is evaluation of the critical distance. Tentatively, when both b and x are heavier than or equal to ^{4}He, we will evaluate R_c in the same way as in Ref.9:

$$R_c = (\langle d^2 \rangle)^{1/2} \quad , \tag{4}$$

where

$$A_a \langle r^2 \rangle_{A_a} = A_b \langle r^2 \rangle_{A_b} + A_x \langle r^2 \rangle_{A_x} + \frac{A_b A_x}{A_a} \langle d^2 \rangle, \tag{5}$$

and

$$\langle r^2 \rangle_A = \frac{3}{5} (1.12\ A^{1/3})^2\ (\ 1 + 3.84\ A^{-2/3}). \tag{6}$$

Here, A_i (i=a,b or x) is mass number of i, $\langle r^2 \rangle_A$ is the mean square radius of a nucleus A, representing the spatial size of the nucleus and $\langle d^2 \rangle$ is the mean square distance between b and x in a. For the case that the spatial size of x can be ignored, say, x=p, n etc., we will evaluate R_c by

$$R_c = (\langle r^2 \rangle_{A_b})^{1/2}. \tag{7}$$

The extended Serber model was applied to energy spectra of ^{13}C and ^{12}C emitted at 14° near the classical grazing angle from collisions of ^{14}N on ^{165}Ho at 280 MeV.[10] We have included the distortion of the spectra and deflection of trajectory in the Coulomb field of the entrance and exit channel following the prescription of Ref.11. That is, we replaced E_a and E_b with $E_a - V_c Z_a$ and $E_b - V_c Z_b$, respectively, where E_i is laboratory kinetic energy of i, Z_i is the atomic number of i (i=a or b), and V_c is the Coulomb energy per unit charge. The Coulomb deflection requires replacing θ with $\theta - \theta_o$, where θ_o is the average deflection angle. V_c was taken to be 8 MeV and θ_o to be 14°. The Coulomb field narrowed the spectra by 11% in the full width at half maximum.

The solid curves in Fig.1 show the results of calculations with ε=7.55 MeV and R_c=2.66 fm for ^{13}C and with ε=10.27 MeV and R_c=2.61 fm for ^{12}C. In both cases, R_c was given by Eq.(7) and ε was calculated as if the fragments are in their ground states after dissociation. The dotted curves show the results with R_c=0 fm. A dependence of the calculation on the value of R_c was further investigated as indicated by the dashed curves in Fig.1. Each curve was independently normalized to the data. It should be noted that the introduction of R_c gives rise to a considerable narrowing of the spectra and that the model reproduces the higher energy part of the spectra well, but misses a fairly large

amount of the lower energy part, especially for ^{13}C. This suggests contributions from other reaction mechanisms, for example sequential decay of the excited projectile-like fragments, to the lower energy region of the spectra.

We have also applied the present model to the data of Gelbke et al[12]. The thick solid curves in Fig.2 show the results of calculations of the ^{15}N and ^{12}C spectra from collisions of ^{16}O on ^{208}Pb at 218 MeV and 315 MeV. The R_c for ^{15}N and ^{12}C was determined by Eq.(7) and Eq.(4), respectively, and V_c was taken to be 9 MeV. In the same figure, calculations with the LMPWBA of McVoy and Nemes[4] are also shown for comparison. One can see that the present model reproduces the higher energy part of the spectra and gives similar results to the LMPWBA calculations.

Finally, we should compare the present model with that of Friedman[5]. In order to clarify the diffrence between the two, let us rewite Eq.(2) in a Gaussian form, assuming $p_{//} \ll$ ~~p~~. The assumption holds over a wide range of $p_{//}$. The parallel momentum distribution of the fragments b in the rest frame of a is given in the present model by $\exp(-p_{//}^2/2\sigma^2)$ with

$$\frac{\sigma^2}{(\hbar c)^2} = \frac{\alpha}{2R_c}\left[\left(1+\frac{5}{2}\eta\right)^{-1}\right] \quad , \qquad (8)$$

whereas the Friedman model gives

$$\frac{\sigma^2}{(\hbar c)^2} = \frac{\alpha}{2x_o}\left[(1+\eta)\right] \quad , \qquad (9)$$

where the physical meaning of x_o is essentially the same as R_c, though the x_o has been determined empirically to be $1.2A_b^{1/3}$.[5] In both cases η is given by $\eta^{-1}=\lambda\alpha$ with $\lambda=R_c$ or x_o. Clearly, one can see that even if the same value is used for the critical distance, the present model predicts narrower momentum distribution than the Friedman model because the factor in the square brackets in Eq.(8) is less than 1, while the same factor in Eq.(9) is greater than 1. As an example, the calculated widths σ of the parallel momentum distribution for ^{16}O and ^{12}C from collisions of ^{20}Ne on ^{197}Au at various energies from 7.5 MeV/nucleon to 20 MeV/nucleon are listed in Table I and Table II along with experimental values measured by Egelhaaf et al[1]. Both models give the incident energy dependence of the widths in terms of the Coulomb distortion. The different methods of evaluating the critical distance in the two models does not cause the difference in the results. The Table shows that the values of σ predicted by the present model are consistently smaller than those by the Friedman model. The present model

roughly reproduces the experimental values at the lowest two energies, but underestimate σ at the higher energies.

I would like to thank Dr. W.A. Friedman for valuable discussions. I would also like to thank Dr. N. Takigawa for helpful discussions at the early stage of this work and Dr. D.J. Morrissey for his comments on the manuscript. The work is supported by the National Science Foundation under Grant PHY-83-12245.

APPENDIX A: FOURIER TRANSFORMATION FOR STRIPPING REACTION IN HI PROJECTILE DISSOCIATION

In this appendix, we perform Fourier transformation of the intrinsic wave function $\psi_{b-x}(\vec{r})$ under the condition needed for the stripping reaction in heavy ion projectile dissociation. Because of the assumption that the constituents loose their identities inside the critical distance, the wave function can schematically be described as shown in Fig.3. The behavior of $\psi_{b-x}(\vec{r})$ at $r \geq R_c$ is governed by the Yukawa wave function, while its amplitude is quickly damped ar $r < R_c$. If we take, for simplicity, a sharp cut-off approximation, that is,

$$\psi_{b-x}(\vec{r}) \propto \begin{cases} \dfrac{e^{-\alpha r}}{r} & r \geq R_c \\ 0 & r < R_c \end{cases}, \qquad (A1)$$

then the Fourier transform $\psi(\vec{p})$ for a transparent target nucleus is given by

$$\psi(\vec{p}) \propto \int_{R_c}^{\infty} \psi_{b-x}(\vec{r})\, e^{-\frac{i}{\hbar}\vec{p}\cdot\vec{r}}\, d\vec{r}$$

$$\propto \frac{e^{-\alpha R_c}}{(\alpha^2\hbar^2 + p^2)} \left(\cos\frac{p}{\hbar}R_c + \frac{\alpha\hbar}{p}\sin\frac{p}{\hbar}R_c\right). \qquad (A2)$$

For the transparent target nucleus, the breakup fragments are considered to never be disturbed by the target and go into the exit channel.

Following the way of Serber[6], let us formulate the stripping reaction for the opaque target nucleus. We employ the coordinate system, which is shown in Fig.4, as follows. The origin is defined at the edge of the target nucleus. The z axis is chosen in the direction of the beam, x axis perpendicular to the edge, and y axis parallel to the edge. By performing inverse Fourier transformation over p_x, we obtain the wave function $\phi(p_y,p_z,x^b,x^x)$ with position variables x^b for b and x^x for x.

$$\phi(P_y,P_z,x^b,x^x) \propto \int_{-\infty}^{\infty} dP_x' \psi(P_x',P_y,P_z)\, e^{\frac{i}{\hbar}P_x'(x^b-x^x)} \qquad (A3)$$

We now impose the condition for the stripping reaction. That is, b misses the target ($x^b \geq 0$) but x hits ($x^x \leq 0$). The result $\Phi(p_y,p_z,p_x,p_x^x)$ is expressed in terms of three cartesian components p_x, p_y, and p_z for b and x component p_x^x for x as follows:

$$\Phi(P_y,P_z,P_x,P_x^x) \propto \iint_{\substack{x^b\geq 0\\ x^x\leq 0}} dx^b dx^x\, \phi(P_y,P_z,x^b,x^x) \times e^{-\frac{i}{\hbar}(P_x x^b + P_x^x x^x)} \qquad (A4)$$

We estimate the integral in Eq.(A4) in the following approxmation. (i) We require the minimum separation R_c for the x coordinates of b and x, i.e., $x^b - x^x \geq R_c$ instead of requiring the separation for the distance between them. (ii) We replace the integration area (Region I+II+III in Fig.5) defined by $x^b - x^x \geq R_c$, $x^b \geq 0$ and $x^x \leq 0$ with the area (Region II in Fig.5) defined by $x^b \geq R_b$ and $x^x \leq -R_x$, where $R_b + R_x = R_c$, i.e.,

$$\iint_{\substack{x^b - x^x \geq R_c \\ x^b \geq 0 \\ x^x \leq 0}} dx^b dx^x \cdots \rightarrow \int_{R_b}^{\infty} dx^b \int_{-\infty}^{-R_x} dx^x \cdots \quad . \tag{A5}$$

Substituting Eq.(A2) into Eq.(A5), we find

$$\Phi(P_y, P_z, P_z, P_x^x) \propto \frac{e^{-\frac{R_c}{\hbar} P} \; e^{-\frac{i}{\hbar} P_z R_b} \; e^{\frac{i}{\hbar} P_x^x R_x}}{P(P_z - iP)(P_x^x + iP)} , \tag{A6}$$

where $P = (\alpha^2 \hbar^2 + p_y^2 + p_z^2)^{1/2}$. The probability, $w(\vec{p})$, that the momentum of b is found in the interval of $\vec{p} \sim \vec{p} + d\vec{p}$ is

$$w(\vec{p}) = \int_{-\infty}^{\infty} dp_x^x \left| \Phi(p_y, p_z, p_x, p_x^x) \right|^2$$

$$\propto \frac{e^{-2\frac{R_c}{\hbar} P}}{P^3 (p_x^2 + P^2)} \quad . \qquad (A7)$$

The laboratory momentum $\vec{p}_b$ of b is given by the coupling of the intrinsic momentum $\vec{p}$ and the momentum $\vec{p}_o$ due to the incident motion of the projectile. Algebraically, $p^2 = p_b^2 + p_o^2 - 2p_b p_o \cos(\theta)$, where θ is the laboratory angle. p_z is nothing but the parallel momentum $p_{//}$ and $(p_x^2+p_y^2)^{1/2}$ gives the transverse momentum $p_\perp$, i.e.,

$$p_{//} \equiv p_z = p_b \cos\theta - p_o$$

$$p_\perp \equiv (p_x^2 + p_y^2)^{1/2} = p_b \sin\theta \quad . \qquad (A8)$$

APPENDIX B: DOUBLE DIFFERENTIAL CROSS SECTION

Since Equation (A7) represents the probability per unit length of the circumference of the target nucleus, we have to integrate $w(\vec{p})$ along

the circumference to obtain the double differential cross section. In Fig.4, $p_y = p_\perp \sin\xi$, where ξ is an angle that defines the position of the origin on the circumference. The double differential cross section $d^2\sigma/d\Omega_b dE_b$ is

$$\frac{d^2\sigma}{d\Omega_b dE_b} \propto A_b P_b \int_0^{2\pi} w(\vec{p})\, d\xi$$

$$\propto \frac{A_b P_b}{(\alpha^2\hbar^2 + p^2)} \int_0^{2\pi} \frac{e^{-2\frac{R_c}{\hbar}(\alpha^2\hbar^2 + P_{//}^2 + P_\perp^2 \sin^2\xi)^{1/2}}}{(\alpha^2\hbar^2 + P_{//}^2 + P_\perp^2 \sin^2\xi)^{3/2}}\, d\xi . \quad \text{(B1)}$$

Here, $p_{//}$ and $p_\perp$ are related to the laboratory angle Θ and momentum p_b by Eq.(A8). Because $w(\vec{p})$ for each unit length of the circumference contributes equally to the parallel momentum distribution, we find Equation (3), which is obviously obtained by substituting $p_\perp = 0$ ($\Theta = 0$) into Eq.(B1).

References

[1] Ch. Egelhaaf et al., Phys. Rev. Lett. 46 813(1981).

[2] M.J. Murphy and R.G. Stokstad, Phys. Rev. C28 428(1983).

[3] A.S. Goldhaber, Phys. Lett. 53B 306(1974).

[4] K.W. McVoy and M.C. Nemes, Z. Physik A295 177(1983).

[5] W.A. Friedman, Phys. Rev. C27 569(1983).

[6] R. Serber, Phys. Rev. 72 1008(1947).

[7] N. Matsuoka et al., Nucl. Phys. A311 173(1978).

[8] J.R. Wu, C.C. Chang, and H.D. Holmgren, Phys. Rev. Lett. 40 1013(1978).

[9] T. Matsuse, A. Arima, and S.M. Lee, Phys. Rev. C26 2338(1982).

[10] H. Utsunomiya et al., Proc. the INS-RIKEN International Symposium on Heavy-Ion Physics, Mt. Fuji, Japan, 1984.

[11] H. Utsunomiya, Phys. Rev. C30 1748(1984).

[12] C.K. Gelbke et al., Phys. Report 42 311(1978).

TABLE I. Experimental (σ^{exp}) and calculated widths for parallel momentum distributions of ^{16}O from collisions of ^{20}Ne on ^{197}Au at various bombarding energies.

E/A (MeV)	σ^{exp} (MeV/c)	$\sigma^{1)}$ (MeV/c)	$\sigma^{2)}$ (MeV/c)
20	66	48	77
14.5	64	45	70
11.0	46	42	64
7.5	37	34	48

1) present work with ε=4.73 MeV, V_c=9 MeV and R_c=2.90 fm.
2) by the Friedman model with ε=4.73 MeV and x_o=3.02 fm.

TABLE II. Experimental (σ^{exp}) and calculated widths for parallel momentum distributions of ^{12}C from collisions of ^{20}Ne on ^{197}Au at various bombarding energies.

E/A (MeV)	σ^{exp} (MeV/c)	$\sigma^{1)}$ (MeV/c)	$\sigma^{2)}$ (MeV/c)
20	94	77	103
14.5	90	72	94
11.0	70	67	88
7.5	67	55	66

1) present work with ε=11.98 MeV, V_c=9 MeV and R_c=2.87 fm.
2) by the Friedman model with ε=11.98 MeV and x_o=2.75 fm.

Figure Captions

FIG.1 Comparison of ^{12}C and ^{13}C spectra from collisions of ^{14}N on ^{165}Ho at 280 MeV with the results of the present model. The solid curves stand for calculations with R_c=2.66 fm for ^{13}C and R_c=2.61 fm for ^{12}C. A dependence of the calculation on the value of R_c is shown by the dotted curves (R_c=0.0 fm) and the dashed curves (short-dashed curve: R_c=1.0 fm, long-dashed curve: R_c=10.0 fm in each case). Experimental data are shown by the solid circles.

FIG.2 Comparison of the results between the present model and the local-momentum PWBA in Ref.4 for ^{15}N and ^{12}C spectra from Ref.12. The thick solid curves and the thin solid curves denote the results of the present model and the local-momentum PWBA calculations, respectively.

FIG.3 Schematic plot of the intrinsic wave function.

FIG.4 Coordinate system

FIG.5 Integration area in the x^b - x^x plane. R_c is the critical distance. R_b and R_x are defined so that $R_b + R_x = R_c$. The point U can be anywhere on the segment ST.

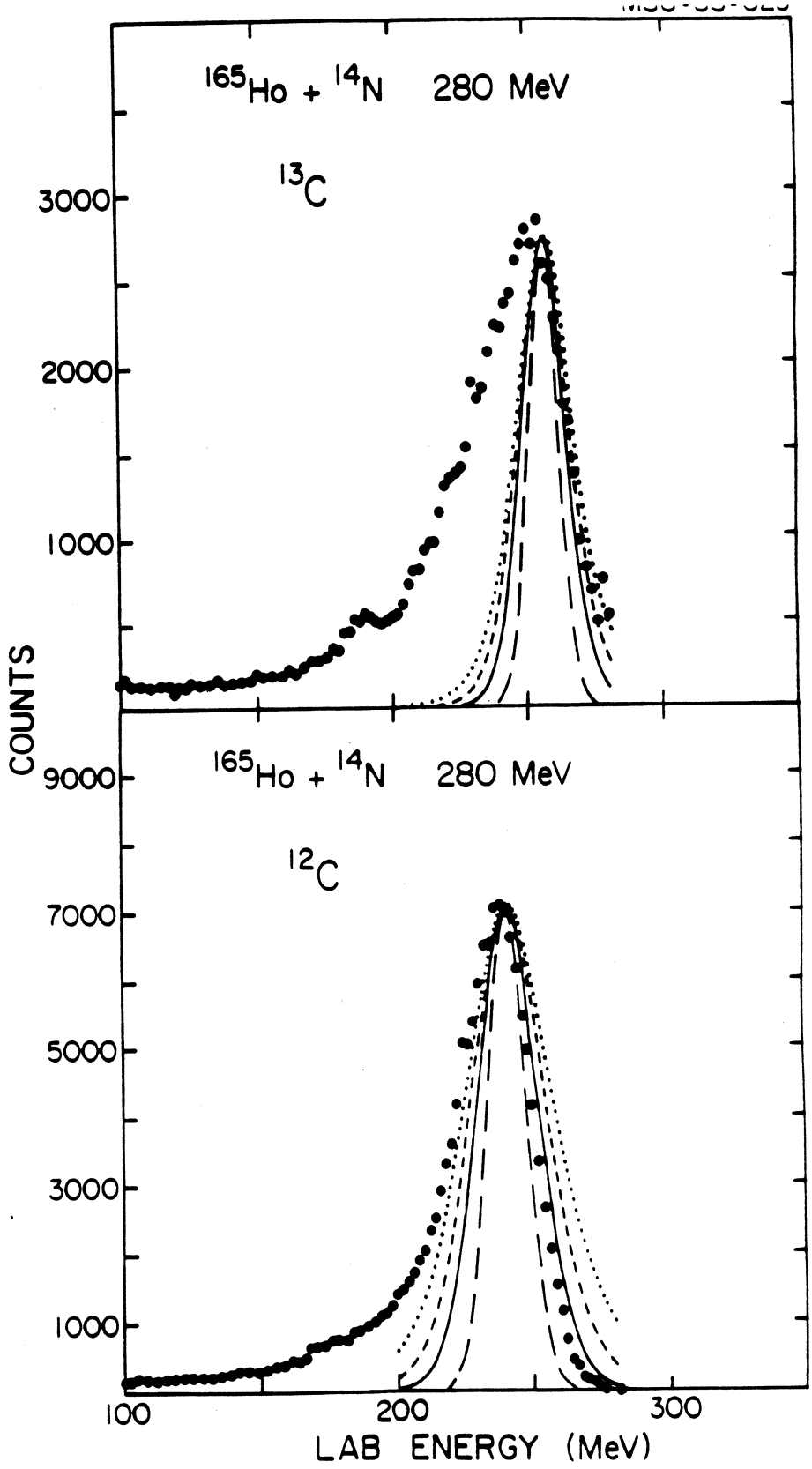
^{165}Ho + ^{14}N 280 MeV
^{13}C
3000
2000
1000
COUNTS
^{165}Ho + ^{14}N 280 MeV
^{12}C
9000
7000
5000
3000
1000
100
200
300
LAB ENERGY (MeV)

Fig. 1

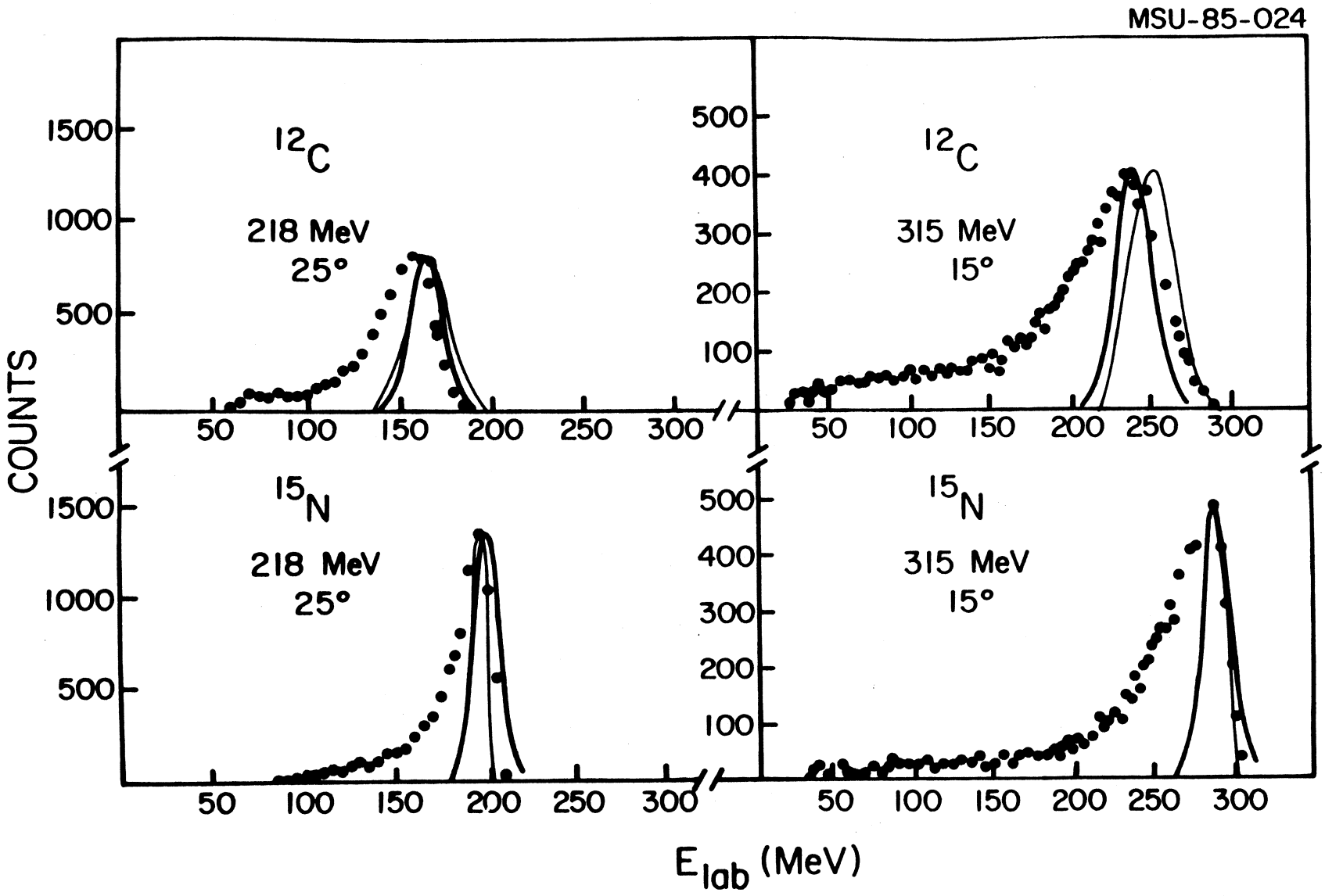
MSU-85-024
^{12}C
218 MeV
25°
^{12}C
315 MeV
15°
^{15}N
218 MeV
25°
^{15}N
315 MeV
15°
COUNTS
E_{lab} (MeV)

Fig. 2

MSU-85-078

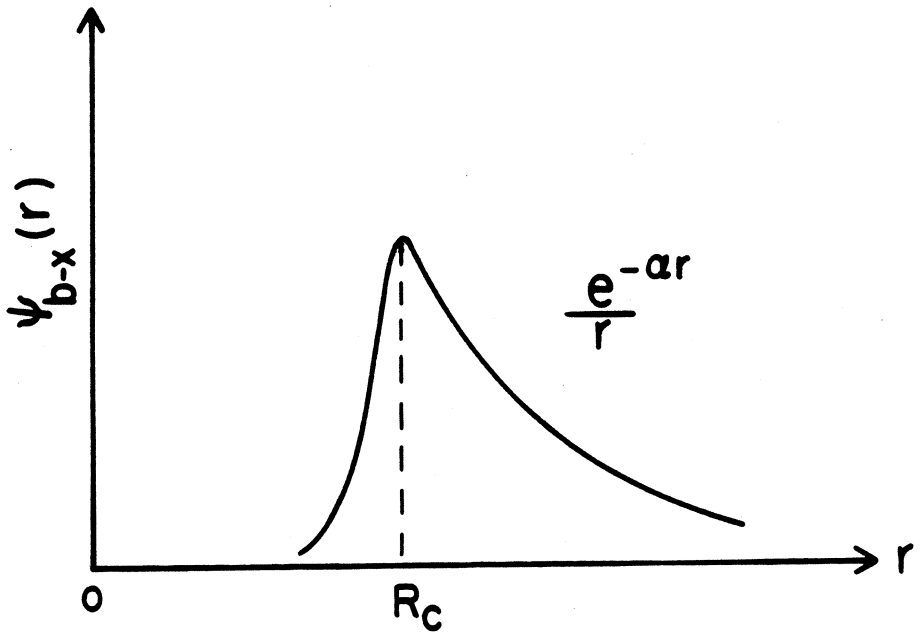

Fig. 3

MSU-85-079

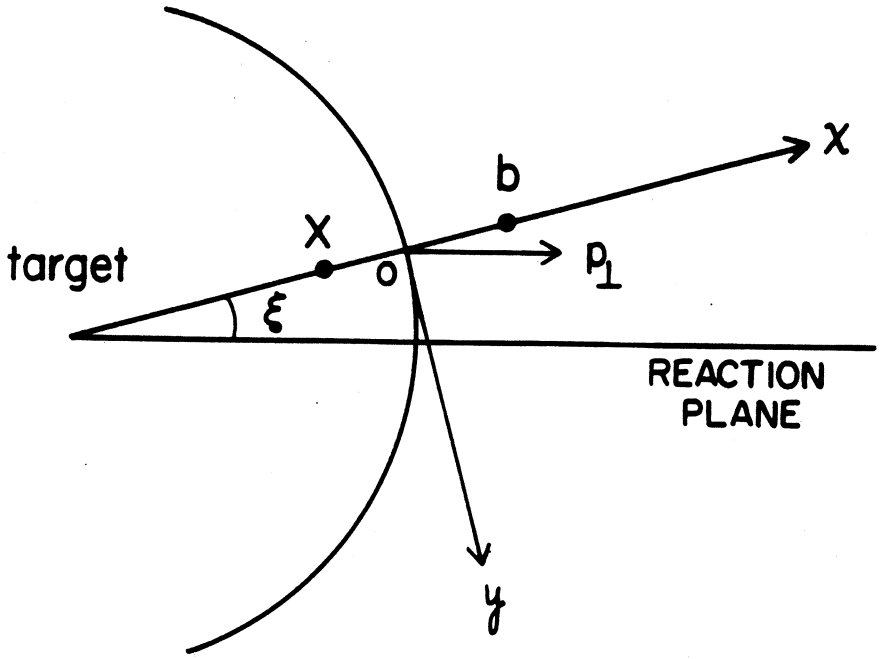

Fig. 4

MSU-85-080

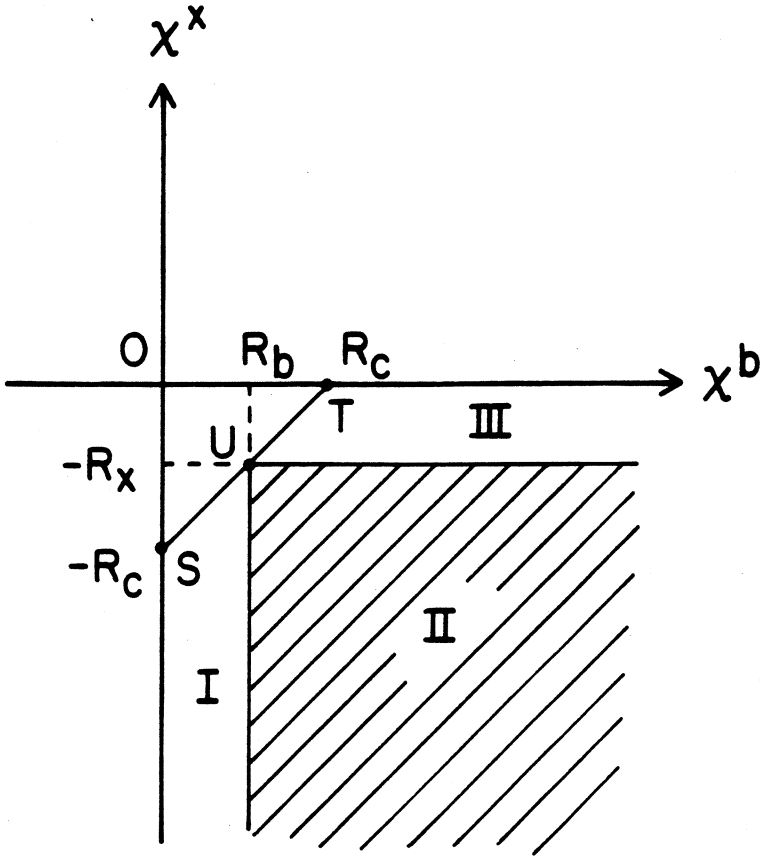

Fig. 5